Real-time diagnostics of gas/water assisted injection molding using integrated ultrasonic sensors

Mulvaney-Johnson, L.; Cheng, C. C.; Ono, Y.; Brown, E. C.; Jen, C. K.; Coates, P. D.

Publisher's version / Version de l'éditeur:
https://doi.org/10.1179/174328907X177617
Plastics, Rubber and Composites: Macromolecular Engineering, 36, 3, pp. 111-121, 2007-04-01

Real time diagnostics of gas/water assisted injection moulding using integrated ultrasonic sensors

L. Mulvaney-Johnson*[1], C. C. Cheng[2,3], Y. Ono[4], E. C. Brown[1], C. K. Jen[5] and P. D. Coates[1]

An ultrasound sensor system has been applied to the mould of both the water and gas assisted injection moulding processes. The mould has a cavity wall mounted pressure sensor and instrumentation to monitor the injection moulding machine. Two ultrasound sensors are used to monitor the arrival of the fluid (gas or water) bubble tip through the detection of reflected ultrasound energy from the fluid polymer boundary and the fluid bubble tip velocity through the polymer melt is estimated. The polymer contact with the cavity wall is observed through the reflected ultrasound energy from that boundary. A theoretically based estimation of the residual wall thickness is made using the ultrasound reflection from the fluid (gas or water) polymer boundary while the samples are still inside the mould and a good correlation with a physical measurement is observed.

Keywords: Gas assisted injection moulding, Water assisted injection moulding, Ultrasound, Process management

Introduction

The area of fluid assisted polymer processing covers both single and two phase fluid/polymer combinations; this work is concerned with the two phase gas and water assisted injection moulding processes. The two phase implementation of fluid assisted moulding typically utilises either gas or water as the fluid and there is a distinct boundary between the fluid and the polymer melt; a single bubble is intended to form therefore leaving the article hollow. The advantages of both gas and water assisted moulding are very similar and both can be utilised to manufacture thick sectioned items by gas or water penetration through the melt to 'core out' the article. Gas assisted moulding has been in existence for many years and has been utilised to manufacture items such as suitcase handles, grab handles and make rib junctions hollow. More recently, water assisted moulding has developed to increase the heat transfer from the moulten polymer to the fluid, which potentially can reduce product cycle time. In addition, the water process has typically realised smoother internal surface finish and thinner residual wall. The foaming of the inner wall often observed with gas assist is thought to be caused by the dissolution of the gas into the melt that later precipitates, when the gas pressure is released, to form local surface foam. The improved internal surface finish from the water process offers the potential to form media ducts where the risk of particulate break off has been minimised and viscous drag reduced. The main advantages of the water and gas assisted moulding processes over the conventional injection moulding process include the ability to provide an even and reduced pressure distribution within the mould during cooling, which can reduce post-moulding warpage for reasons previously outlined, reduction in outer surface 'sink' due to the expansion of the pressurised fluid bubble internally as the polymer melt shrinks upon cooling and good thermal contact with the cavity wall resulting from the prolonged cavity pressure; material savings can be realised in the 'short shot' process configuration.[1,2]

A further variation of the gas assisted moulding process is the application of gas between the mould wall and polymer melt. This configuration usually requires the mould to be gas sealed to contain the gas pressure within the mould. The gas is applied to the non-aesthetic surface of the product, which may contain strengthening ribs, and is used to push melt against the aesthetic surface of the mould. This has the effect of improving the aesthetic surface finish and reducing the 'witness' marks opposite the rib junctions. The even distribution of a lower melt pressure within the cavity, when compared with the conventional process, typically results in lower residual stress and therefore reduced warpage.[3]

[1]IRC in Polymer Science and Technology, University of Bradford, Bradford, BD7 1DP, UK
[2]Deptartment of Electrical and Computer Engineering, McGill University, Montreal, Que., Canada
[3]Deptartment of Electrical Engineering, Hsiuping Institute of Technology, Da-Li, Taichung, Taiwan
[4]Deptartment of Systems and Computer Engineering, Carleton University, Ottawa, Ont., Canada
[5]Industrial Materials Institute, National Research Council Canada, Boucherville, Que., Canada

*Corresponding author, email l.johnson@Bradford.ac.uk

Published by Maney on behalf of the Institute
Received 5 January 2007; accepted 13 March 2007
DOI 10.1179/174328907X177617

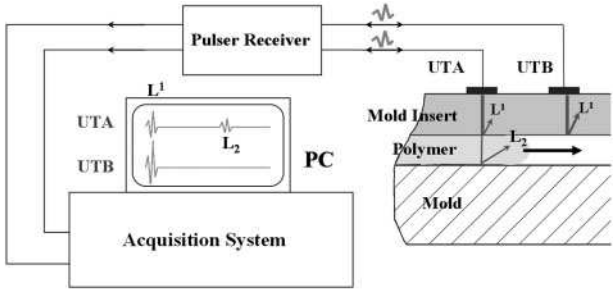

1 Cross-sectional schematic view of mould with UTs and data acquisition system for ultrasonic diagnostics of injection moulding process using ultrasonic pulse echo technique

The work presented here focuses upon the two phase water and gas assisted injection moulding processes. The injection moulding machine and the mould tool are fitted with instrumentation, including ultrasound, to monitor the progress of the melt and water/gas as it penetrates through the melt in a fixed section of the cavity. The test specimen is a long flow path tube with an initial ϕ20 mm and then ϕ10 mm section that is 'cored out' using the gas or water assist. The test specimen is representative of the thick section tubular components that the gas assist process has been used to manufacture. The applications for water assisted components have been noted in literature to be automotive media ducts, door handles and thick sectioned components of a child's tricycle.[4,5]

Method of mould based ultrasonic diagnostics and sensors

Ultrasonic signatures such as propagation characteristics (velocity and attenuation), reflection and transmission coefficients, and scattering signals from materials, are associated with physical and rheological properties of materials (phase, viscosity, microstructure, chemical composition, density, molecular weight, filler concentration, etc.), process dynamics (cycle, injection, packing, holding, cooling, mould open, ejection, etc.), material dynamics (melting, flow arrival and advancement, filling completeness, solidification, shrinkage, detachment, etc.), process parameters (temperature, pressure, etc.) and product qualities (uniformity, shape, surface flatness, deformation, inclusions, voids, etc.). Thus, these signatures can be used for diagnostics of polymer processes and product quality.[6–13] For such purposes, ultrasonic transducers (UTs) are attached onto the extrusion barrel and/or mould (mould insert) of injection moulding machines.

Figure 1 shows a cross-sectional schematic view of a conventional injection moulding tool fitted with the UTs and data acquisition system using an ultrasonic pulse echo technique. Ultrasonic waves radiated from the UTs propagate through both the mould insert and polymer, and reflections at the material interfaces within the propagation paths are received by the same UTs. Echoes L^n (where n=1, 2, 3, etc.) are the nth round trip longitudinal echo reflected at the nearest cavity wall interface. This interface is either steel/air or steel/polymer, depending on if polymer has arrived at that location. Echoes L_n (where n=1, 2, 3, etc.) are the nth round trip longitudinal echo from the furthest polymer/steel interface. Both the time delay and amplitude variations of these echoes are used to measure the ultrasonic velocity and signal attenuation through the steel and polymer materials. The steel conditions are relatively constant and the propagation of the ultrasound signal within the polymer is related to local pressure and temperature, which in turn reflects the process conditions. A multiple sensor configuration enables monitoring of the melt flow in the mould cavity and polymer status at the chosen locations. The ultrasonic data acquisition system was composed of two pulser receivers (Panametrics Inc., Waltham, MA, USA), a 12 bit dual channel digitising boards (Gage Applied Science Inc., Montreal, Que., Canada) with a sampling rate of 50 MHz for each channel and a personal computer with a data acquisition and analysis program by LabVIEW. The data acquisition rate of analysed values from each ultrasound generated waveform was 100 Hz.

The developed high temperature ultrasonic transducer (HTUT) has overcome some of the key practical issues and limitations for application to industrial polymer processes at elevated temperatures.[14,15] Limitations include the degradation of couplant between the transducer and the steel surface along with the need for a cooling system for the transducer, which adds complexity to the application and could induce thermal changes to the process. Three piezoelectric HTUT sensors were directly integrated onto a mould insert of a gas/water assisted injection moulding machine (TM1300 from Battenfeld). The polymer side of the mould insert had a half cylindrical cavity with a radius of 10 mm and three UTs (UT-A, -B and -C) were fabricated at the HTUT side with an interval of 35 mm, as shown in Fig. 2*a* and *b* respectively. Figure 2*c* presents a moulded part with an inset of a cross-section of the part at the UT-A area, where three black dots indicate the corresponding areas of the UTs. These UTs had a centre frequency of 9 MHz and 6 dB bandwidth of 6 MHz. Figure 3 presented the performances of UT-A. L^n (n=1, 2) indicates the nth round trip longitudinal echoes propagating in the HTUT sensor insert and reflecting within the mould insert/air interface. Signal to noise ratio (SNR) of the first round trip longitudinal wave echo, reflected at the substrate/air interface measured in pulse echo technique, was above 30 dB at room temperature. In addition, it was confirmed that these sensors could be operated up to 200°C. Such performance is sufficient for monitoring of polymer water/gas injection moulding processes where the mould insert bulk temperature is likely to peak at ~100°C when certain polymeric materials are processed.

Figure 4 presents a schematic cross-section of the gas and water assisted mould with the UTs, showing ultrasonic propagation paths and flows of polymer melt and fluid (gas or water) within the cavity during the moulding cycle. L_S is the longitudinal echo that is reflected from the interface between the 'frozen layer' of polymer near the mould wall and the remaining polymer melt. $L_{G(W)}$ is the longitudinal echo reflected at the liquid/gas (water) interfaces. In Fig. 4, ultrasound partially transmits to water during water assisted injection moulding (WAIM), resulting in less reflected ultrasonic energy when compared with gas assisted moulding; this will be further discussed later.

A cavity sensor with combined pressure and temperature sensing capabilities (Kistler type 6190 A) was flush

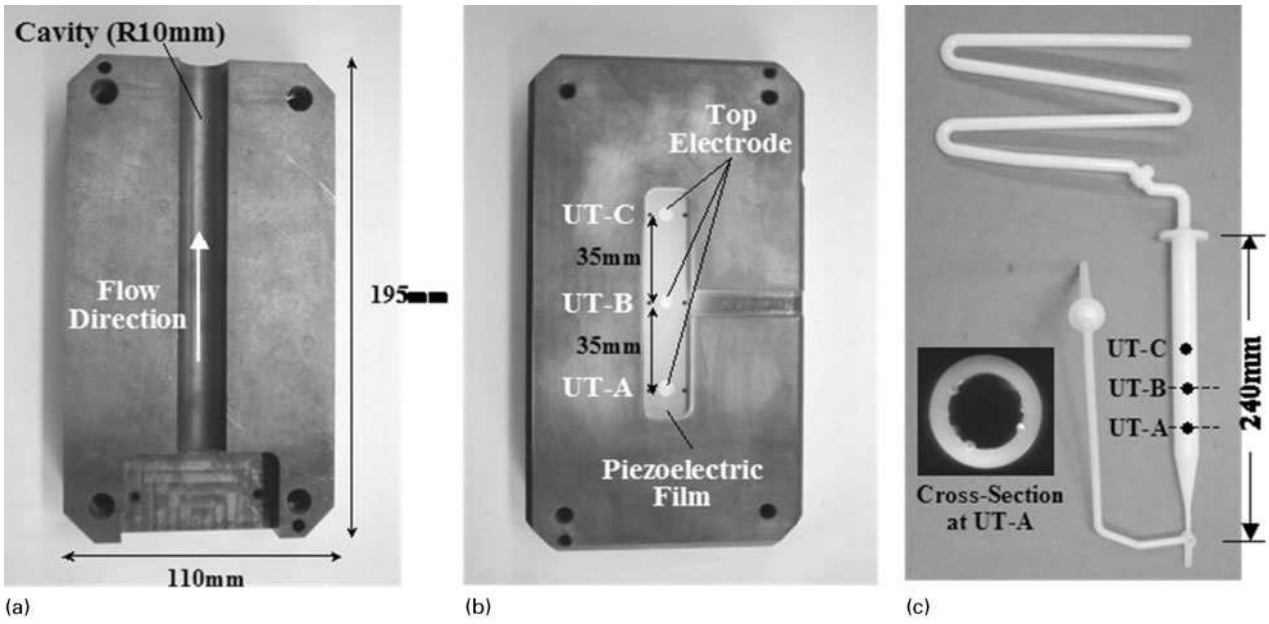

2 Photographs of *a* polymer side of mould insert having half cylindrical cavity with radius of 10 mm, *b* three HTUTs (UT-A, -B and -C) fabricated on opposite side of cavity and *c* moulded part, with gas/water assisted injection moulding

mounted to the mould cavity in a location opposite the UT-B transducer. This arrangement allowed for the polymer temperature and pressure at the mould wall to be measured for comparison with the ultrasonic data; Fig. 4 shows schematically the positioning of the transducers.

Experimental

The gas and water assisted injection moulding processes were operated on an injection moulding machine at the University of Bradford, Bradford, UK. The injection moulding machine, shown in Fig. 5, was a Battenfeld TM1300/350+210 BM fitted with a B4 controller. This machine has the capability to deliver two different polymer melts to the mould (skin and core materials), but in this case, only one of the available injection barrels was utilised as only a single material was required. The Barrel A is ϕ40 mm internal diameter with a maximum specific melt pressure of 160 MPa and maximum melt delivery rate of 132 ccm s^{-1}.

A specially designed mould tool was utilised for preparation of the gas and water assisted samples, and a photograph of the actual tool mounted on the machine platens is shown in Fig. 6. The tool is comprised of a main cavity plate that houses inserts containing the mould cavity form and exchange of the cavity inserts allows for different forms and flow lengths to be studied; the cavity form was not changed for the work presented here. The polymer melt is injected into the cavity at the location shown and follows a runner to the bottom of the tool where the fluid injection needle is located. The needle is located at the bottom of the tool, which is a requirement for successful extraction of the water using gravity at the end of the moulding cycle. Shown in Fig. 6 is the insert containing the instrumented straight ϕ20 mm tubular region of the sample. This section is instrumented with pressure, temperature and ultrasound transducers that coincide in position along the section to provide data from the same locations. The combined pressure and temperature transducer (close-up of ϕ4 mm sensor shown in Fig. 6) is positioned at the same

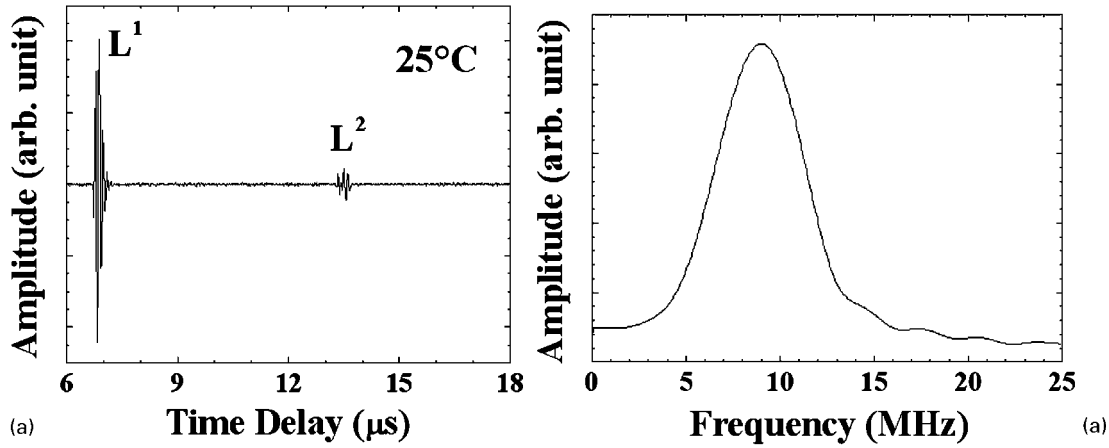

3 Performance of ultrasonic sensor UT-A *a* in time and *b* in frequency domain at room temperature

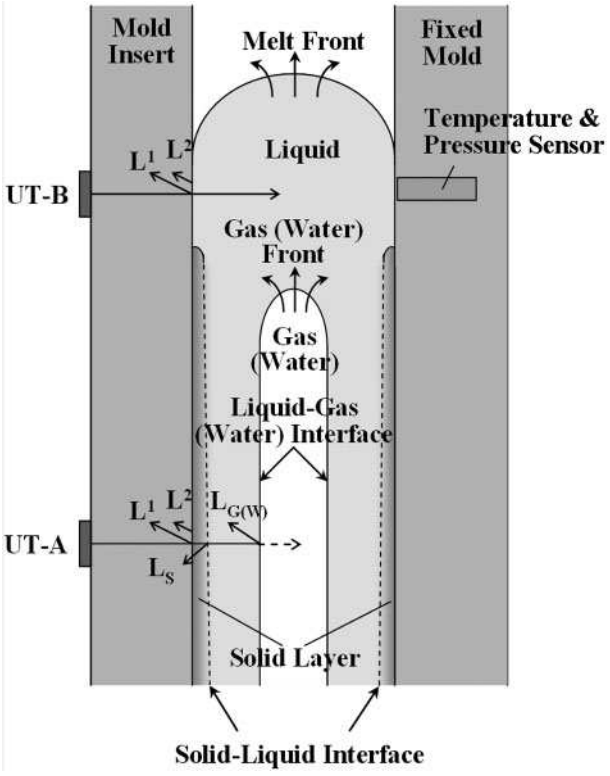

4 Schematic cross-section of mould with UTs with ultrasonic propagation paths and flows of polymer melt and fluid (gas or water) in cavity, with gas/water assisted injection moulding

location along the tube specimen and opposite to the ultrasound transducer 'B'; ultrasound transducers and their locations are discussed later.

The 'short shot' method was used to manufacture these specimens, where the mould cavity is partially filled with polymer (the short shot) before the injection of either gas or water. The fluid bubble displaces the polymer melt to the end of the cavity in order to complete filling and the final specimen becomes hollow with either a gas or water core, depending upon the process. Before the mould opening, the high pressure gas or water is released from the mould to leave a hollow article.

5 Battenfeld injection moulding machine with separate gas/water injection controller shown in foreground: water injection reservoir is shown behind machine

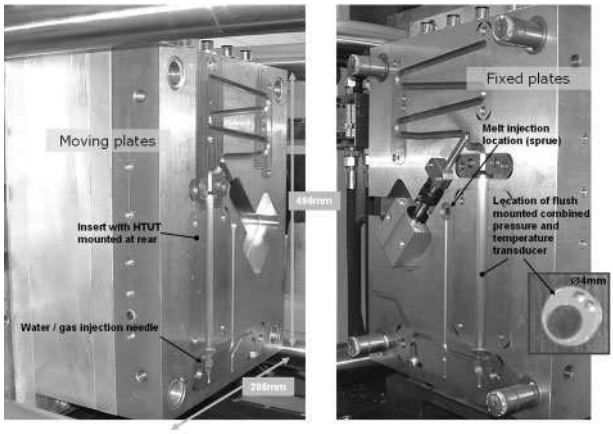

6 Combined water and gas assist moulding tool showing cavity form that is made up from interchangeable inserts: ϕ20 mm straight tube insert fitted with HTUT (moving side) along with combined piezoelectric pressure and thermocouple temperature transducer (fixed side) is shown

The material used here was high density polyethylene from BP chemicals (BP Rigidex HD5050EA), which has good ultrasound propagation properties. Single melt and mould temperature settings of 250 and 30°C respectively were used throughout and these are the mid point settings suggested by the material manufacturer. The melt injection rate was set to be 60 ccm s^{-1} over the entire 135 ccm melt delivery phase. However, because the peak available injection pressure was reached during the melt injection phase, the actual injection rate was measured to be $\sim$40 ccm s^{-1}. The fluid injection pressures were changed in these experiments in order to change the residual wall thickness and therefore bubble front velocity[16–18] if the bubble propagation could be interpreted from the ultrasound data and if changes to the residual wall thickness could be monitored. The gas and water injection pressure settings were 10, 12 and 20 MPa, and 17·5, 20 and 25 MPa respectively. The fluid pressure was increased to the set value in a single step, held for 6·0 s and then the system valves were closed for a further 10 s before the fluid pressure was released.

Results

The experimental results for the gas assisted injection moulding (GAIM) experiments are presented, where specimens were moulded with gas injection pressures of 10, 12 or 20 MPa. Figure 7 shows a typical result of acquired ultrasonic signals from UT-A during one cycle of GAIM using the ultrasonic pulse echo technique. The L^1 and L^2 echoes are clearly marked on the data and correspond to the first and second round trip echoes between the transducer and cavity surface. The L_S and L_G echoes are also clear and correspond to the echo from the frozen layer/polymer melt interface and the polymer melt/gas interface respectively. At around a process time of 9·2 s, the L_G echo starts to appear, indicating that the gas bubble front was first observed at the UT-A location at this time. Both the L_G and L_S echoes remain evident up to a process time of 27 s, at which point the gas pressure is released and the polymer may detach from the cavity wall. Detachment from the

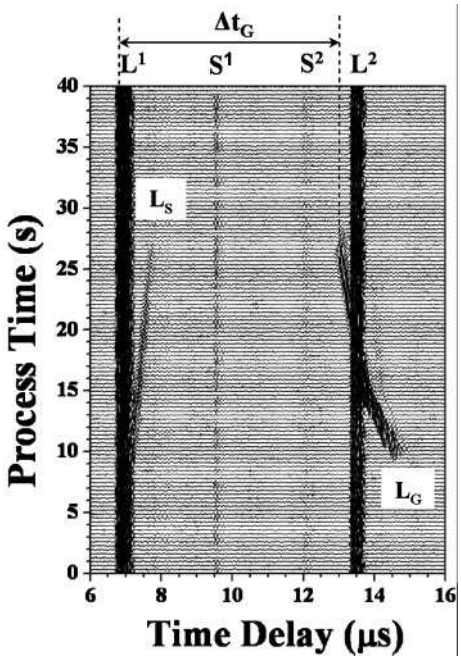

7 Typical signals acquired during one cycle of gas assisted injection moulding process

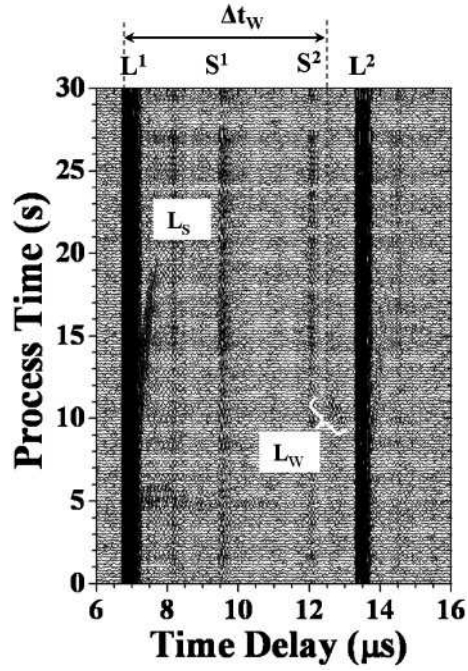

8 Typical signals acquired during one cycle of water assisted injection moulding process

cavity wall is driven by the shrinkage of the polymer during cooling and associated phase change. The changing time delay of the L_S and L_G echoes may be evidence that the polymer was still in the melt phase during this time. In the process time from 9 to 27 s, the time delay of the L_G echo varied from 14·5 to 13 μs, indicating the solidification, temperature reduction of the part and the wall thickness reduction due to the movement of gas bubble. However, in the same period, the variation of the L_S echoes only implied the solidification and temperature reduction of the part. It is noted that the small echoes S^n (n=1, 2) always appearing at the time delay of 9 and 12 μs are the shear wave signals propagating in the mould insert.

Results from a typical water assisted moulding cycle are presented in Fig. 8 where the water injection pressure is 20 MPa. This figure shows the ultrasonic signal data from UT-A with the familiar L^1, L^2 and L_S echoes indicated. The L_W echo appearing around the process time of 10 s with the time delay of ~12·5 μs is an echo reflected from the polymer/water interface. This L_W echo is difficult to detect as the SNR is low, certainly when compared with the L_G echo (gas assist) in Fig. 7. The reason for the difference is a much lower ultrasound reflection coefficient at the polymer/water interface of 0·2 compared with a reflection coefficient of ~1·0 for the polymer/gas interface. In effect, these coefficients indicated that 20% of ultrasound was reflected at the polymer/water interface in WAIM while ~100% (total reflection) of the signal is reflected at the polymer/gas interface.[15] In addition, voids within the wall of water moulded samples were observed scattered and/or attenuated the ultrasonic signals propagating within the wall. Owing to the weak reflected signal from the bubble interface in water assisted moulding, no further comparison work was possible with this body of data.

In order to investigate further the correlation between the ultrasonic signals observed and the gas assisted moulding cycle, a process time based comparison is made between the amplitude values of the L^2 and LG echoes (Fig. 7) and the gas pressure control signal and cavity wall pressure at the UT-B location. Results showing the L^2 and L_G echoes with respect to process time are presented in Fig. 9. The gas pressure control signal and cavity wall pressure with respect to process time are shown in Fig. 10. The L^2 echo was chosen instead of the L^1 echo because in principle, higher order round trip echoes of L^n can lead to a higher sensitivity to the cavity wall interface condition.[19] In Fig. 9, at process time of 6·3 s, the polymer melt arrived at the cavity area beneath the UT-A, because the amplitude of the L^2 echo decreased as an increasing proportion of the ultrasonic energy was transmitted into the polymer through the cavity wall/polymer interface. Figure 10 shows that around this time, the cavity pressure started to increase, indicating arrival of the polymer melt at the UT-B location. Thus average polymer melt speed V_m during this melt injection phase can be estimated from the time difference Δt_m between the fall in L^2 echo amplitude at UT-A and the increase in the cavity pressure at the UT-B location by equation (1)

$$V_m = \frac{L}{\Delta t_m} \quad (1)$$

where L=35 mm and is the distance between the UT-A and UT-B locations.

The average polymer melt speed is ~175 mm s^{-1}; however, other process signals contradict this value of melt front velocity, which is discussed later.

At 8·3 s (Fig. 10), the gas injection control signal begins to rise, which corresponds to the injection of gas at the gas needle. The amplitude of the L_G echo increases significantly at 9·2 s (Fig. 9), which indicates that the gas bubble interface with the melt has suddenly appeared at the UT-A location. The L_G echo amplitude stays high, but the L_G signal becomes indeterminate when its transit time coincides with that of the L^2 echo

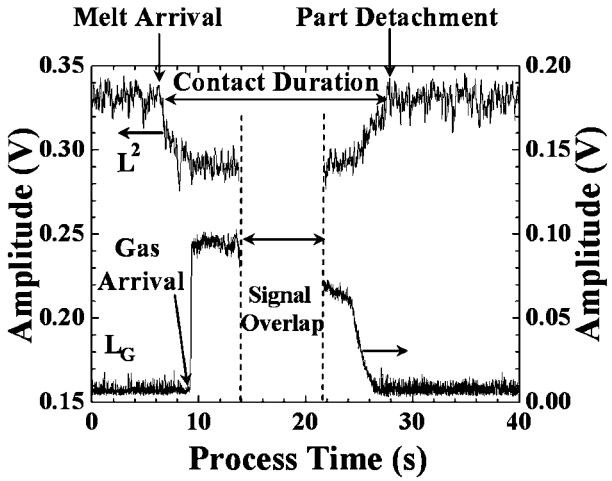

9 Amplitude variations of L^2 and L_G echoes, measured by UT-A with respect to process time

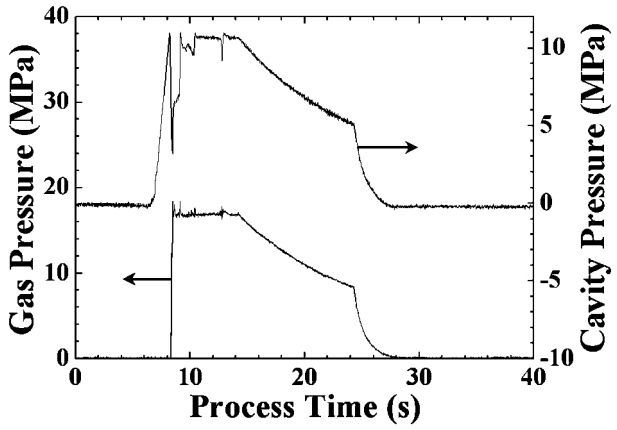

10 Amplitude variations of gas pressure, supplied by gas machine, and cavity pressure, measured by pressure sensor facing to UT-B, with respect to process time

due to signal superposition between 13·8 and 21·7 s of process time. The amplitudes of the L^2 and L_G echoes have been blanked out during this time interval in Fig. 9 and this particular phenomenon can be seen more clearly in Fig. 7.

In Fig. 10, from 6·5 to ~8·0 s, the steady rise in cavity wall pressure is due to the melt prefilling phase. Once melt prefilling is complete, the cavity wall pressure falls rapidly until gas injection takes place at 8·3 s (the associated gas injection control signal rises at this time). From 8·3 to ~10·5 s, the cavity pressure rises during gas bubble penetration and the equalising of pressure across the needle (between the line supply and the gas bubble). The set gas pressure is maintained for 6·0 s and then from a process time of 14·0 to 24 s, the gas valves are closed during a period termed 'vent delay time'. The cavity pressure during this vent delay time gradually falls as the gas bubble volume increases due to melt shrinkage and escape of gas from the system (probably through the needle/polymer seal that forms). At 27·5 s, the amplitudes of both the L^2 and LG echoes recovered to their initial values as the gas pressure was released from the system. This infers that the polymer has detached from the cavity wall because the condition at the cavity wall for ultrasound is the same as that at $t=0$, i.e. no melt present. The detachment of the specimen from the mould wall is not unexpected as shrinkage of the polymer during cooling is known to take place. The process time from 6·3 (the amplitude of the L^2 echo decreased) to 27·5 s (the amplitude of the L^2 echo recovered to the initial value), was called 'ultrasonic contact duration'. The contact duration may indicate the period during which the specimen and mould are in contact and helps to evaluate the cooling efficiency. This information will be discussed further in the section 'External diameter distribution'.

Discussion

Melt prefilling

Melt prefilling or short shot, provides a known quantity of polymer melt to the cavity before the injection of either gas or water. Because the movement of the melt injection piston or screw has been recorded during this melt injection phase, an estimate of the melt injection rate can be made. Assuming incompressibility of the polymer melt and no back flow of polymer over the piston during its forward movement, then the rate of piston volumetric displacement is equal to the volumetric flow rate within the ϕ20 mm section of the mould cavity, where the UT-A, UT-B and pressure transducers are located. Figure 11 shows two process signals, which are melt volume in front of the melt injection piston and cavity wall pressure at location UT-B taken from the Kistler piezoelectric pressure transducer. The third signal plotted in Fig. 11 is rate of change of melt volume in front of the injection piston, which is differentiated from the volume signal already plotted. The rise in cavity wall pressure at UT-B is noted in Fig. 11 and corresponds to an increase in melt pressure at that point. If the melt was flowing in the usual fountain flow regime, this pressure rise would indicate the arrival of the melt flow front, as shown schematically within this figure. The melt volume between the UT-A and UT-B locations is 11 ccm and the time taken for the injection piston to deliver this is 0·5 s, therefore, the average volumetric flowrate is 22 ccm s^{-1}. The corresponding average melt flow front velocity between UT-A and UT-B, which are 35 mm apart, is therefore 70 mm s^{-1}. It is worth noting at this point that the set volumetric flowrate of the piston was 60 ccm s^{-1}, but due to the required injection pressure being above 80% of that available from the machine (160 MPa), the actual injection rate was lower.

Examination of the UT-A and UT-B signal amplitude data reveals that the actual melt front velocity is apparently much higher than that calculated from the movement of the melt injection piston. Figure 12 shows a fall in the amplitude of the L^2 echo upon arrival of the polymer melt at each of the UT-A and UT-B transducer sites. The second plot shows the corresponding cavity wall pressure rise at the UT-B site. The time difference between these apparent melt arrival events is ~0·15 s, which would give a corresponding melt flowrate of 73 ccm s^{-1} and melt front velocity of 233 mm s^{-1}. The melt flowrate determined from this data is higher than even the machine set point of 60 ccm s^{-1}.

A photograph of a solidified specimen that was not water or gas injection moulded is shown in Fig. 13. This specimen indicates how the melt prefilling pattern may

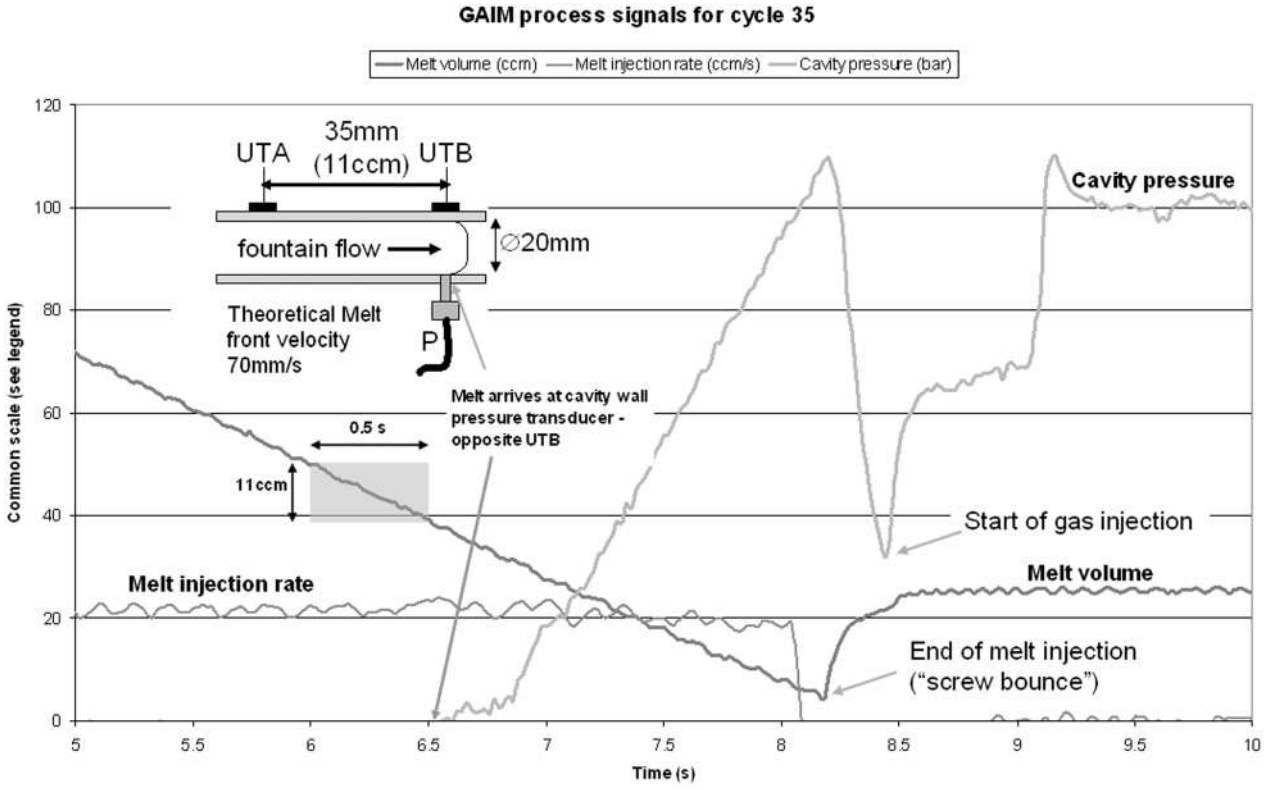

11 Process signals showing displacement of melt injection screw (falling melt volume in front of screw), rate of melt delivery to mould and cavity wall pressure at UT-B location

look and the 'spiraling' effect points towards melt 'jetting' during this prefilling phase. The jetting phenomenon, in this case, is due to the polymer melt not maintaining contact with the cavity wall as it passes from the relatively narrow ϕ4 mm gate into the much larger ϕ20 mm section. During jetting, the polymer may be thrown forwards ahead of the theoretical melt flow front position to make contact with the cavity wall in the UT-A and UT-B locations. However, in order for ultrasonic energy to be transmitted in to the polymer melt, certain pressure and satisfactory contact are necessary so that the UT can have the sensitivity to detect such ultrasonic energy transmission. During jetting, the melt contacts the mould surface randomly and may not touch sensing areas of the UTs. Furthermore, even the melt contacts the sensing area of the UT, but may be in a condition that ultrasonic energy was not transmitted into the polymer melt through mould insert/polymer melt interface sufficiently for the UT to detect. Therefore, during the jetting process under the experimental conditions, the recorded ultrasonic signals did not have enough sensitivity to show the 'contact' and 'non-contact' situation.

The reasons for the apparent discrepancy between the flowrate of melt into the mould from the machine barrel and the apparent flowrate of melt in the cavity within the ϕ20 mm section are not fully resolved in this work, although jetting is believed to be a significant contributing factor.

Gas flow speed

Tracking the flow front speed of the gas bubble over moulding cycles may present an opportunity to detect needle blockages or reductions in gas supply pressure to the mould. Figure 14 presents the amplitude variations

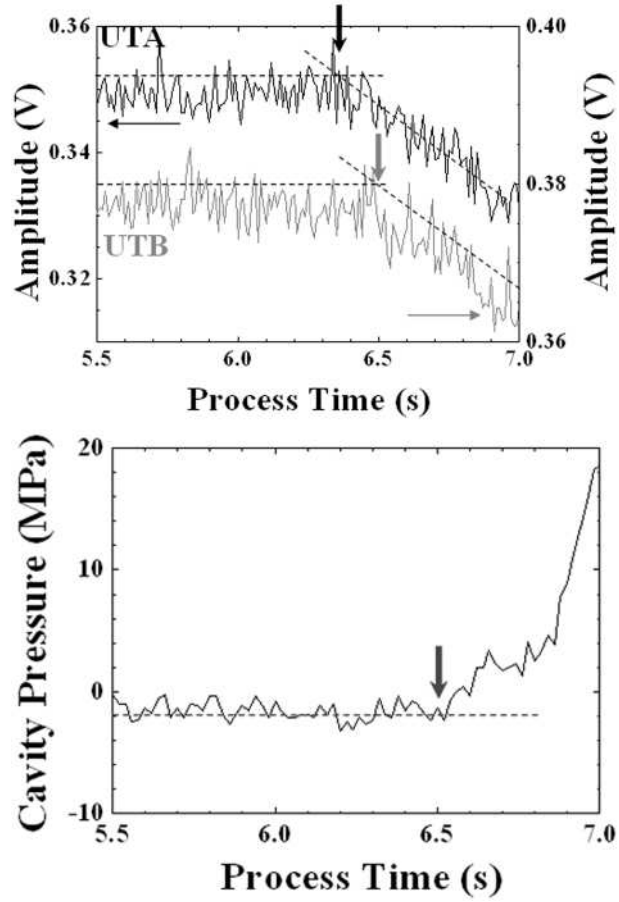

12 Melt arrival at cavity wall is denoted by fall in UT signal amplitude: signal amplitude for UT-A and UT-B is shown; cavity pressure at same location along specimen as UT-B increases as the melt passes over transducer

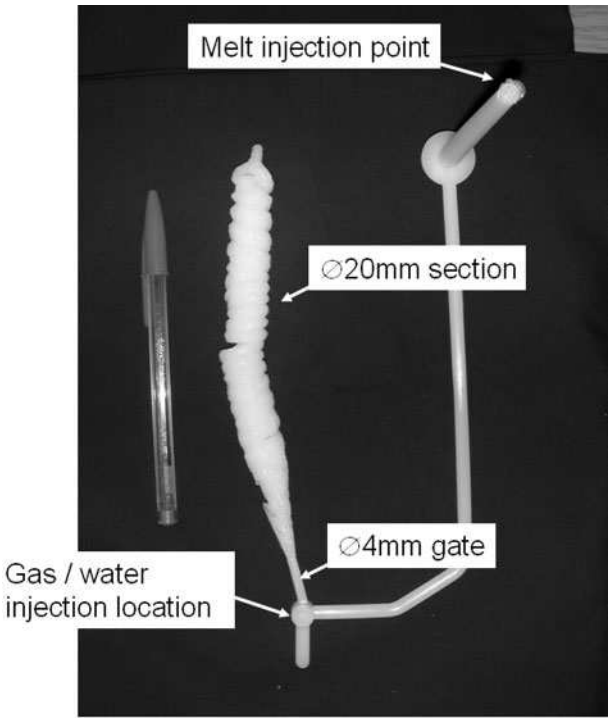

13 Form of melt at end of melt prefilling and before injection of gas or water: coiled form clearly indicates that 'jetting' of polymer melt from ϕ4 mm gate has taken place within ϕ20 mm section of cavity

of the L_G echoes, measured by UT-A and UT-B, with respect to the process time. The L_G echoes began to be observed at 9·2 and 9·7 s with the UT-A and UT-B respectively, when gas arrived at each UT location. Therefore, gas flow speed V_f could be estimated using the time differences Δt_f of appearances of the L_G echoes at the UT-A and UT-B locations by

$$V_f = \frac{L}{\Delta t_f}$$

where L (35 mm) is the distance between the UT-A and UT-B. The results are presented in Fig. 15. Gas flow speed increased with gas pressure. The bubble speed is linked to the formation of the relative wall thickness (RWT), where higher speed (higher pressure) results in a thinner RWT. In addition, these data provide valuable insights into the actual processing conditions that can be utilised to validate the results from mould filling simulations.

Wall thickness

Quality control to evaluate the wall thickness of the moulded part is crucial for fluid assisted injection moulding. But currently, the measuring method was limited to offline techniques, in which the parts are cut to measure the wall thickness. Thus, real time ultrasonic thickness measurement of the parts was conducted during fluid assisted injection moulding process. After moulding, the moulded parts were sectioned and a thickness gauge, with the accuracy of ± 1 μm, was used to measure wall thickness at the locations corresponding to the UT-A and UT-B positions in Fig. 2. The measuring results of wall thickness for gas/water assisted injection moulding are shown in Figs. 16 and 17 respectively. In these two figures, the closed squares

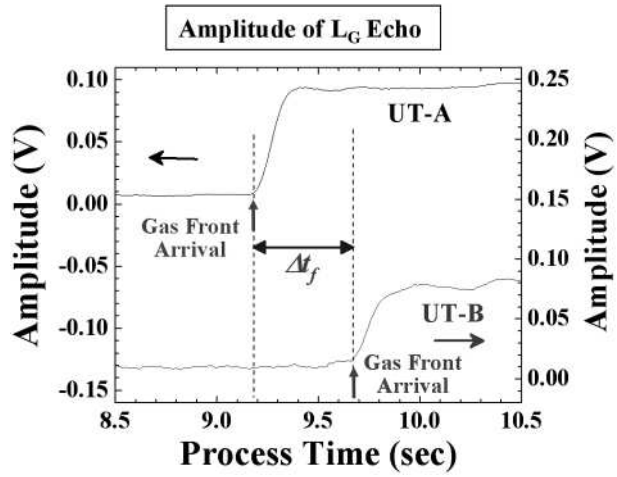

14 Amplitude variations of L_G echoes, measured by UT-A and UT-B, with respect to process time: rapid increase in amplitudes indicates gas front arrival at each UT location

(■) and circles (●) indicated the measured wall thickness by a thickness gauge at the UT-A and UT-B areas respectively. The wall thicknesses at the UT-B (●) were greater than those at the UT-A (■) close to the gas/water injection nozzle, except for part no. 9 in Fig. 16 and part no. 2 in Fig. 17. This anomaly is thought to be an end effect because the UT-A location is close to the tapered transition section where gas flowrate is expected to be unsteady or the unsteady water flow when the water pressure was low.

The wall thicknesses were estimated by equation (2)

$$h_m = \frac{1}{2} V \Delta t_m \quad m = G, W \tag{2}$$

where h_m is wall thickness estimation in mm, V is ultrasonic velocity in the polymer, and Δt_G and Δt_W are the time delay difference between L^1–L_G and L^1–L_W in Figs. 7 and 8 respectively. The time delay differences of Δt_G and Δt_W were chosen at the process time of 27·0 s in Fig. 7 and 11.0 s in Fig. 8 respectively. These timings were just before the L_G and L_W echoes disappeared. In the estimation, the ultrasonic velocities of 1108 and 1297 m s^{-1} in the polymer just before the part

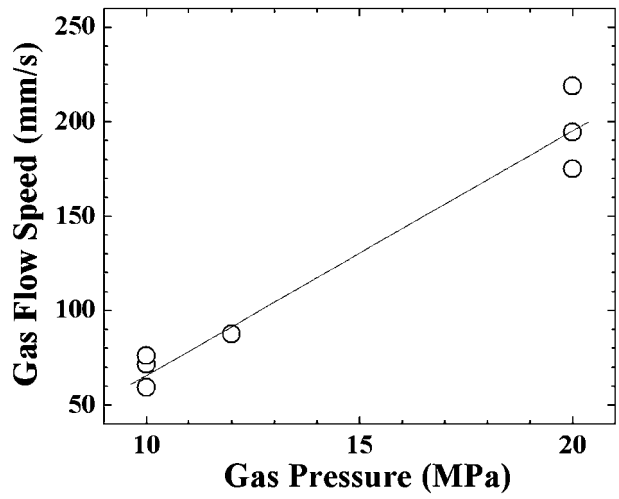

15 Gas flow speed between UT-A and UT-B measured by ultrasonic technique with different gas pressures

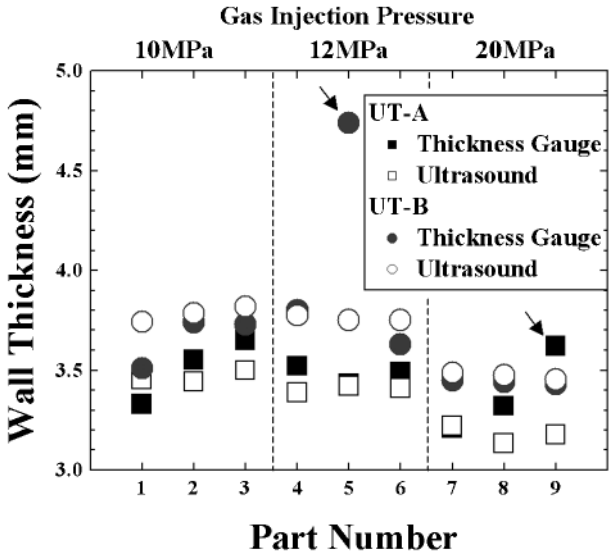

16 Comparison of wall thicknesses measured by thickness gauge after sectioning parts and those estimated by ultrasonic technique during moulding with different gas pressures

detachment were used to calculate the wall thicknesses for gas/water assisted injection moulding respectively. These velocities were obtained using the time delay differences and the measured wall thicknesses at 20 MPa. The estimations of wall thickness using the ultrasound data are given in Figs. 16 and 17 with open squares (□) and circles (○) to indicate UT-A and UT-B respectively. It is noted that in Fig. 17, parts nos. 1, 4 and 5 cannot provide estimated wall thicknesses at UT-B, and part no. 5 cannot provide that at UT-A. In Fig. 16, the measured and estimated wall thicknesses had good agreement within an accuracy of $\pm 7\%$ except for the parts no. 5 at the UT-B and no. 9 at the UT-A, indicated by the arrows. In Fig. 17, the agreement was within an accuracy of $\pm 10\%$ except for the part no. 2 at the UT-B, indicated by the arrow. This suggests that water bubble inclusions within the residual wall may have provided an early echo that appeared to be a thinner than actual residual wall.

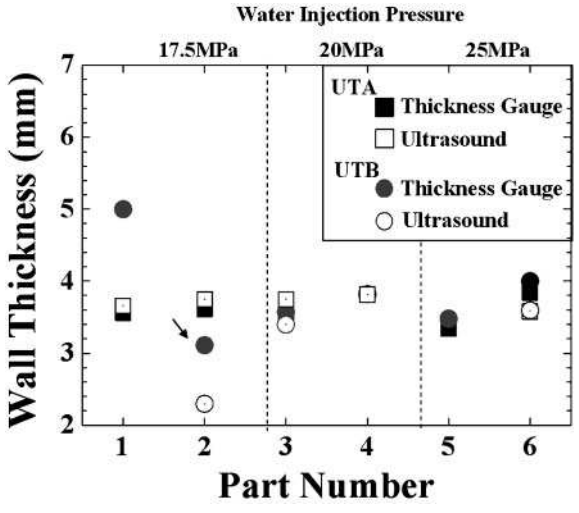

17 Comparison of wall thicknesses measured by thickness gauge after sectioning parts and those estimated by ultrasonic technique during moulding with different water pressures

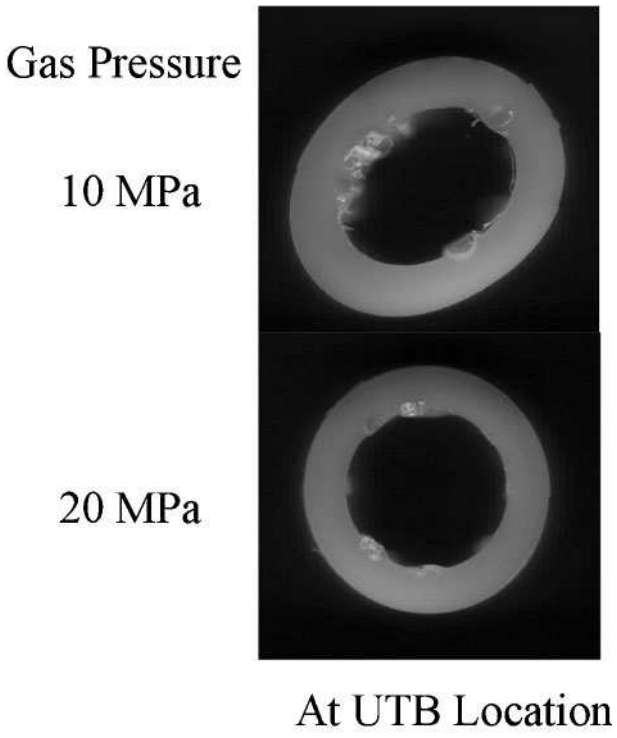

18 Photograph of sectioned parts at UTB location with respect to gas pressure of 10 and 20 MPa

External diameter distribution

Fluid assisted injection moulding incorporated gas or water injection in the mould filling cycle to form the hollow components. Therefore, to keep the hollow structure from deformation is the basic requirement for part quality. In the authors' experiments, the gas/water was injected into the mould during the filling process with the pressure of 10, 12 and 20 MPa, and 17·5, 20 and 25 MPa respectively. In order to understand the correlation between the formed hollow structure and the injected gas/water pressure, two parts with gas pressure of 10 and 20 MPa were sectioned in the UT-B location. Figure 18 presents the photograph of these two sectioned parts. It is clearly seen that the part with gas pressure of 10 MPa has a serious deformation and more bubbles existing in the inner surface of the hollow structure. But the part with gas pressure of 20 MPa presents a uniform shape and fewer bubbles.

Here, the external diameter distribution, a parameter indicating the level of deformation for the moulded hollow structure, was presented with gas/water injection pressure. The external diameter distribution can be calculated by

$$\frac{D_{\max} - D_{\min}}{D_{\min}} \times 100\%$$

where $D_{\max}$ and $D_{\min}$ were the external maximum and minimum diameters in each UT location. A calliper, with accuracy of $\pm 0{\cdot}02$ mm, was used to measure the diameter. The measured diameter distributions in UT-A, -B and -C location, indicated by square (■), circle (●) and triangle (▲) respectively, with respect to the gas pressure, were presented in Fig. 19. The diameter distributions in three UT locations were less than 1% when the gas pressure was 20 MPa. However, those were from

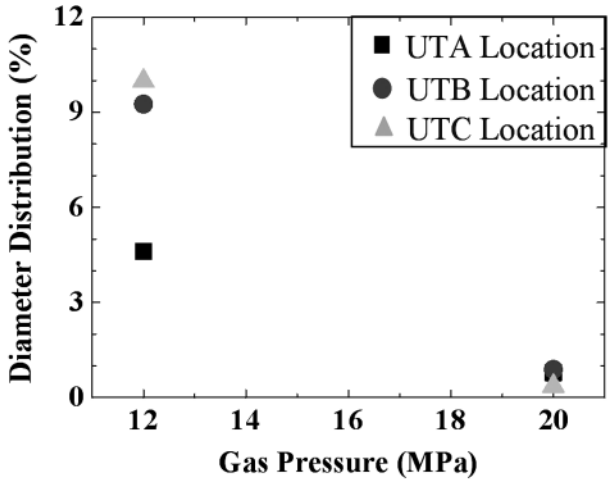

19 External diameter distribution of moulded parts at UT-A, -B and -C locations with respect to different gas pressures in gas assisted injection mould process

4·6 to 9·9%, with respect to UT-A to UT-C location respectively, when the gas pressure was 12 MPa.

Ultrasonic contact duration may also present the relationship between the cooling efficiency and external diameter distribution. Figures 20 and 21 present the ultrasonic contact duration with respect to different liquid (gas or water) pressures in gas/water assisted injection moulding process. Ultrasonic contact duration increases with liquid pressure (gas or water), except part no. 31 (10 MPa) and part no. 41 (20 MPa) indicated by arrows in Fig. 20. When the liquid (gas or water) pressure was less than 20 MPa, the contact duration was not stable and lower. The contact durations of WAIM are less than GAIM, indicating that the cooling efficiency of water is higher than that of gas. These results showed that insufficient gas pressure would cause insufficient cooling for moulded part, part deform during cooling and/or part detachment, and the deformed level would increase with the distance from the gas/water nozzle. In addition, these data provide valuable insights into the actual processing conditions that can be utilised to validate the results from mould filling simulations.

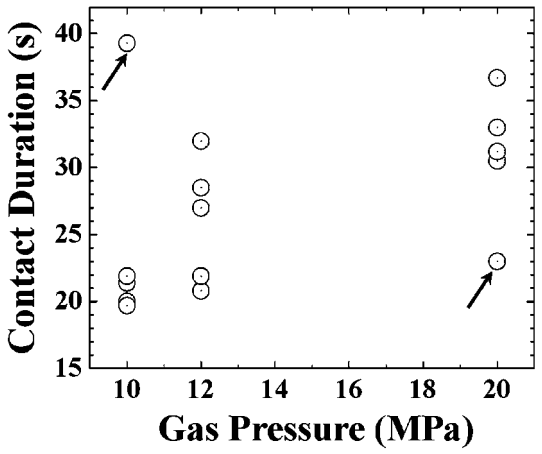

20 Ultrasonic contact time measured by UT-B, during gas assisted injection moulding process, with respect to different gas pressures

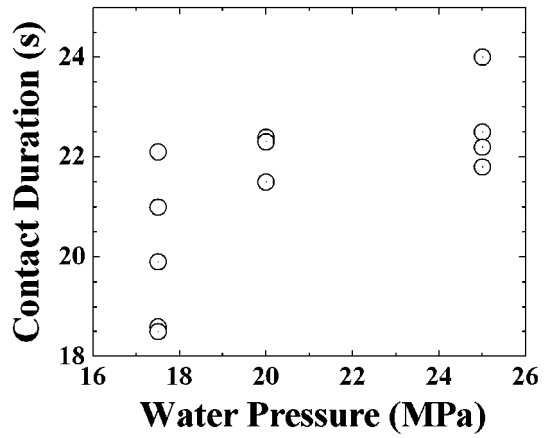

21 Ultrasonic contact time measured by UT-B, during water assisted injection moulding process, with respect to different water pressures

Conclusions

A non-invasive ultrasound sensor system has been applied to the mould for both gas and water assisted injection moulding. The system has successfully detected both the arrival of polymer melt and the arrival of either the gas or water bubble that penetrates through the moulten polymer. A cavity mounted pressure transducer validated the introduction of gas or water into the cavity and changes in the ultrasound energy transmission into the melt along with echoes from the fluid polymer boundary were observed. The strength of reflected ultrasound energy from the fluid polymer interface is the highest for the gas assisted case where the echo can clearly be detected. However, although the strength of reflection from the polymer water boundary is detectable, it is weak and difficult for the automated signal processing system to pick out.

The utilisation of two ultrasound sensors allowed for the progression of the gas bubble through the polymer melt to be detected as the bubble arrival at each sensor location could be detected. The bubble arrival at each sensor also allowed for an estimation of the gas bubble velocity to be made at various gas injection pressure settings. As the gas pressure setting increased, an expected increase in gas bubble tip velocity between sensor locations was observed.

The ultrasound energy reflected from the cavity boundary increases as the polymer detaches from the cavity wall because the acoustic coupling is impaired. This phenomenon allows for estimation for the length of time that the polymer remains in contact with the cavity wall. The cavity wall contact time was observed to be longer and more consistent with the higher fluid pressure settings. A higher post-moulding deformation of the samples was observable where lower fluid pressure settings had been utilised.

The ultrasound data were used to estimate the residual wall thickness while the sample was in the mould. A reasonable correlation was made between the ultrasound estimate and the measured thickness using a Vernier thickness gauge after the sample components were sectioned. Some scatter of the ultrasound thickness data was observed from the water assisted samples due to the inclusion of water voids within the residual wall.

Acknowledgements

The authors would like to the support from EPSRC, Battenfeld UK and GmbH, A. Schulman Polymers, BP Chemicals and Kistler sensors.

References

1. J. Zhao, X. Lu, L. Fong and H. H. Chiang: *SPE ANTEC Tech. Papers*, 1998, **44**, 454–459.
2. S. Y. Yang and S. J. Liou: *SPE ANTEC Tech. Papers*, 1994, **40**, 404–407.
3. T. Pearson: *Mater. World*, 1995, **3**, (3), 119–121.
4. M. Knights: Available at: http://www.ptonline.com/articles/200509fa1.html (accessed September 2005).
5. H. Eckardt: Proc. Polymer Process Engineering Conf., Bradford, UK, June 2001, University of Bradford, 121–155.
6. L. Piché, A. Hamel, R. Gendron, M. Dumoulin and J. Tatibouët: US Patent 5 433 112, 1995, USA.
7. C. L. Thomas, A. A. Tseng, J. L. Rose and A. J. Bur: *SPE ANTEC Tech. Papers*, 1993, **39**, 143–148.
8. C. L. Thomas, A. O. Adebo and A. J. Bur: *SPE ANTEC Tech. Papers*, 1994, **40**, 2236–2239.
9. C. L. Thomas, M. Jiang, C. C. Chen and A. J. Bur: *SPE ANTEC Tech. Papers*, 1995, **41**, 2707–2714.
10. S.-S. L. Wen, C.-K. Jen and K. T. Nguyen: *Int. Polym. Process.*, 1999, **XIV**, 175–182.
11. E. C. Brown, T. L. D. Collins, A. J. Dawson, P. Olley and P. D. Coates: *J. Reinf. Plast. Comp.*, 1999, **18**, 331–338.
12. Y. Ono, C.-C. Cheng, M. Kobayashi and C.-K. Jen: *Polym. Eng. Sci.*, 2005, **45**, 606–612.
13. M. Kobayashi and C.-K. Jen: *Smart Mater. Struct.*, 2004, **13**, 951–956.
14. M. Kobayashi, Y. Ono, C.-K. Jen and C.-C. Cheng: *IEEE Sens. J.*, 2006, **6**, 55–62.
15. A. R. Selfridge: *IEEE Trans. Son. Ultrason.*, 1985, **SU-32**, (3), 381–394.
16. B. G. Cox: *J. Fluid Mech.*, 1962, **14**, 81–96.
17. F. Belblidia, J. F. T. Pittman, A. Polynkin and J. Sienz: *Chem. Eng. Sci.*, 2005, **60**, 4953–4956.
18. P. Olley, L. Mulvaney-Johnson and P. D. Coates: *Plast. Rubber Compos.*, 2006, **35**, (2), 47–58.
19. H. Wang, B. Cao, C. K. Jen, K. T. Nguyen and M. Viens: *Polym. Eng. Sci.*, 1997, **37**, (2), 363–376.